Supporting Information

Theoretical insights into the Activation of Carboplatin and its Interaction with DNA Bases on Magnesia: Synergistic Drug Delivery and Magnesium Supplementation

Zhenjun Song *[ad], Tengfei Huang [b], Longting Song [a], Ting Wang [a], Hongdao Li *[c], Wei Chen *[a], and Guobo Huang [a]

[a] School of Pharmaceutical and Chemical Engineering, Taizhou University, Taizhou 318000, Zhejiang Province, China

[b] Henan Provincial Key Laboratory of Nanocomposites and Applications, Institute of Nanostructured Functional Materials, Huanghe Science and Technology College, Zhengzhou 450006, Henan Province, China

[c] Department of Chemistry and Chemical Engineering, Taiyuan Institute of Technology, Taiyuan 030008, Shanxi Province, China

[d] College of Polymer Science and Engineering, State Key Laboratory of Polymer Materials Engineering, Sichuan University, Chengdu 610065, China

* Corresponding authors. E-mail: songzj@mail.nankai.edu.cn (Zhenjun Song); lihong.dao@163.com (Hongdao Li); wchen@tzc.edu.cn (Wei Chen)

Contents

Models and Methodologies

The calculations on structural optimization, hydrolysis transformation, and electronic properties of carboplatin on magnesia (100) surface are performed utilizing the periodic density-functional theory method with Van der Waals correction DFT-D3(BJ)[1] implemented in Vienna Ab initio Simulation Package[2]. PAW (projector augmented wave) technique is used to treat the atomic core and valence electrons of the carboplatin-magnesia system separately with a full-electron wave function projected onto the pseudo wave function. Generalized gradient approximation (GGA)[3] is used for the description of the electron exchange-correlation term with Perdew–Burke–Ernzerhof (PBE) correction. The cutoff energy for self-consistent field computation is 500 eV, which can expand the wave function with high accuracy. Utilizing Monkhorst-Pack's technique, a 2×2×1 k-point sampling grid is used for the structural optimization of carboplatin and magnesia film. For the properties of charge population, electronic states, electronic localization, and bonding interaction of the carboplatin-magnesia system, the much denser 4×4×1 k-point sampling grid is employed. The stop criterion for electron minimization (ELM) steps is 0.0001 eV for structural relaxation. In contrast, the stop criterion for ELM for static properties is 0.00001 eV.

Due to the deficiency of popular local density functional for predicting dispersion forces, the Van der Waals forces among carboplatin-magnesia (001) system is computed with Becke-Jonson damping, as the following equation,

$$E_{tot} = E_{KS-DFT} + E_{disp} \quad (1)$$

where the E_{tot}, $E_{KS\text{-}DFT}$, and E_{disp} represent total electronic energy, Kohn-Sham DFT energy, and the dispersion energy correction, respectively. For present calculations, the dispersion energy correction is constructed mainly by a two-body term which is calculated by the following expression,

$$E_{corr} = \sum_{AB} \sum_{n=6,8,10,\ldots} s_n \frac{C_n^{AB}}{r_{AB}^n} f_{d,n} r_{AB} \quad (2)$$

where the first sum is over all atom pairs in the carboplatin-magnesia system,

C_n^{AB} represents the *n*th-order dispersion coefficient[4]. All the Hellmann-Feynman residual forces and stress tensors are converged to smaller than 0.02 eV/Å. The large $2\sqrt{2} \times 2\sqrt{2}$ supercell of magnesia (001) is constructed with long surface vectors [1 1 0] and [-1 1 0] of 11.888 Å.

The usage of large magnesia (001) supercell is aimed at avoiding interferential interaction between neighboring carboplatin compound. The adsorption energy E_a is calculated by the following expression,

$$E_a = E(sys) - E(Plat) - E(Mag) \quad (3)$$

where *E*(sys), *E*(Plat), and *E*(Mag) represent the total energy of the system, the energy of the hydrolyzed platinum complex, and the energy of hydroxylated or un-hydroxylated magnesia (001) film, respectively. The reaction energy difference of the carboplatin hydrolysis on magnesia film is calculated by expression,

$$\Delta E = -E_{*car} - 2E_w + E_{le} + E_{*hyd} \quad (4)$$

where the E_{*car}, E_w, E_{le}, and E_{*hyd} are the total energies of the adsorbed carboplatin system, water, leaving group anion, and the adsorbed hydrated diamminoplatinum, respectively.

The frontier molecular orbitals (FMO) of carboplatin-related reaction products are calculated utilizing Gaussian program[5] and BDF program[6-8]. Crystal Orbital Hamilton Populations (COHP) analysis for carboplatin-guanine combination on magnesia film is conducted using the Lobster program developed by Dronskowski's group[9, 10]. Molecular dynamics simulations were conducted in Materials Studio using the Amorphous Cell module[11] to construct the simulation system, followed by geometry optimization in Forcite to achieve structural stability. The composition is 20 Mg^{2+}, 40 $Pt(NH_3)^{2+}$, 40 Cl^-, 40 cyclobutanedicarboxylate ligands and 2000 H_2O molecules. Subsequently, a 1000-ps NVT ensemble equilibration (constant volume and temperature) was performed with randomized initial velocities, a 1-fs time step, and the universal Force Field. During the MD simulation, coordinates and energies were saved every

1000 steps (corresponding to 1 ps). The electrostatics were treated with PPPM method (Particle-Particle Particle-Mesh) for long-range accuracy. Van der Waals interactions were truncated at 12.5 Å with spline smoothing. Electrostatic interactions and temperature control were managed via Ewald summation and the Nosé-Hoover thermostat, respectively, to establish a thermodynamically equilibrated solution system.

Geometric accuracy of the PBE-D3 functional against the OptB88-vdW method and high-level references for platinum complexes

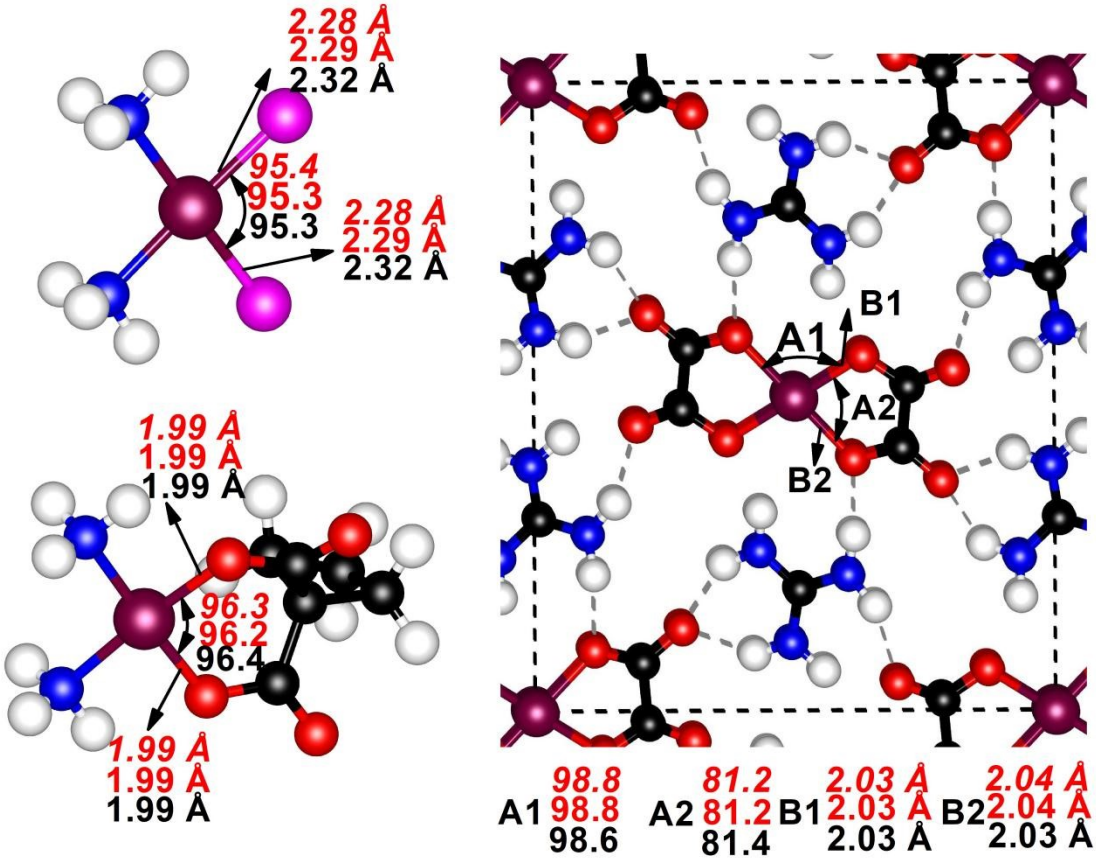

Fig. S1 The geometric accuracy of the PBE-D3 functional against the OptB88-vdW method and high-level references for platinum complexes. Red italic text denotes OptB88-vdW results, red upright text indicates PBE-D3, while black upright text represents the M06-2X (gas phase) or experimental (crystal) reference data. The comparison highlights that PBE-D3 reproduces the reference bond lengths and angles with superior fidelity.

Geometric structures and relative energies for cisplatin adsorption on magnesia (1 0 0) films

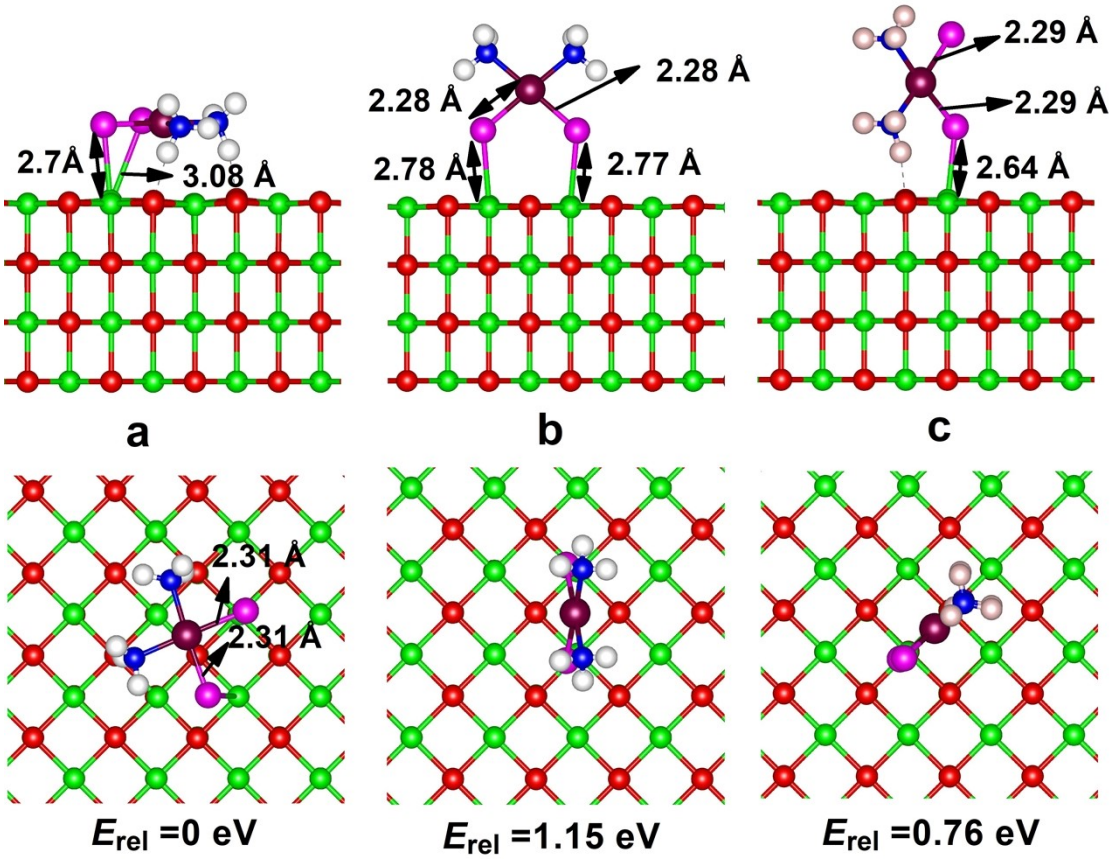

Fig. S2 Geometric structures and relative energies for cisplatin adsorption on magnesia (1 0 0) films.

Differential charge density contour, charge transfer and adsorption energies of cisplatin on magnesia (1 0 0)

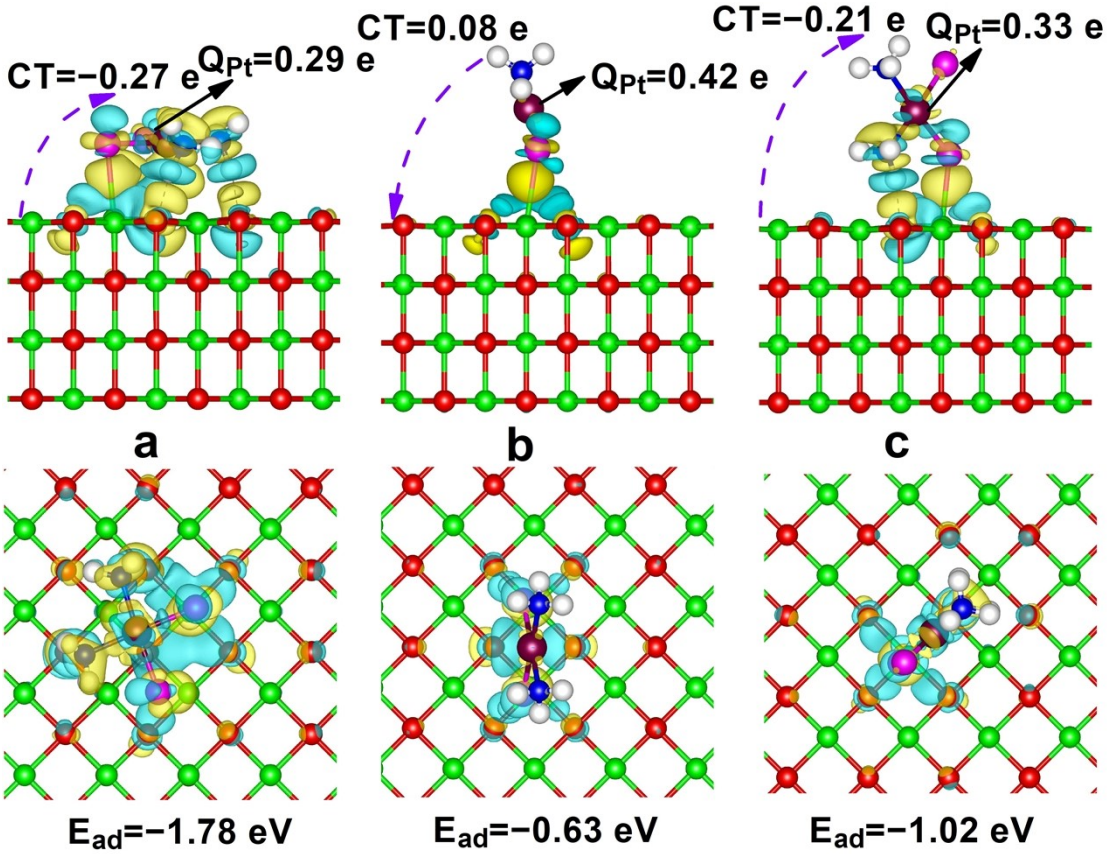

Fig. S3 Differential charge density contour, charge transfer and adsorption energies of cisplatin on magnesia (1 0 0). The yellow and cyan colors represent charge accumulation and charge depletion, respectively. The isosurface value is 0.001 e $Bohr^{-3}$.

ELF, charge density contours and differential charge density (DCD) contours

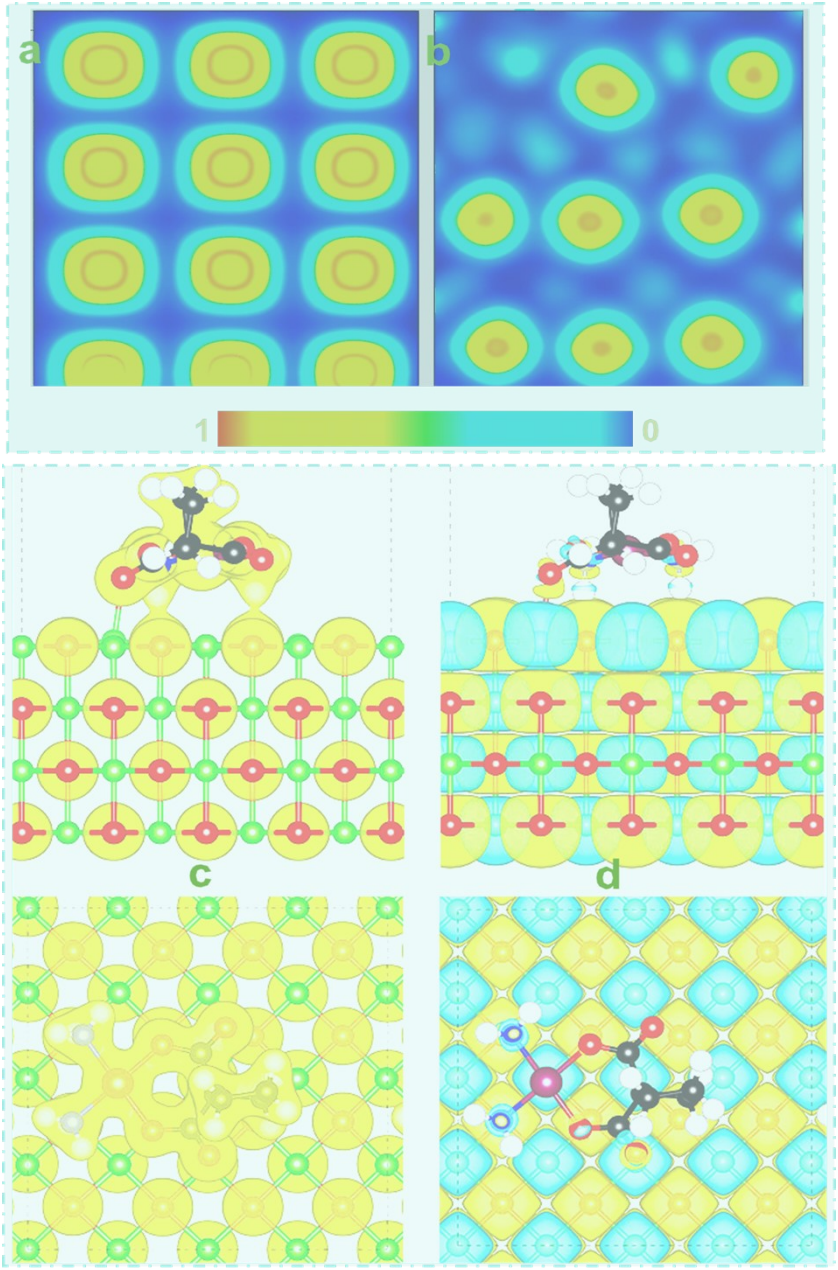

Fig. S4 Electron localization function (ELF) contours for carboplatin adsorbed on MgO(001): (a) along [001], (b) along [010]. Red: electron localization; blue: electron delocalization. Charge density contour (c) and differential charge density (DCD) contour (d). Yellow: charge accumulation; green: charge depletion. Isosurface values: 0.05 e $Bohr^{-3}$ (charge density), 0.005 e $Bohr^{-3}$ (DCD).

The local projected density of states (PDOS) for carboplatin adsorption on magnesia (001)

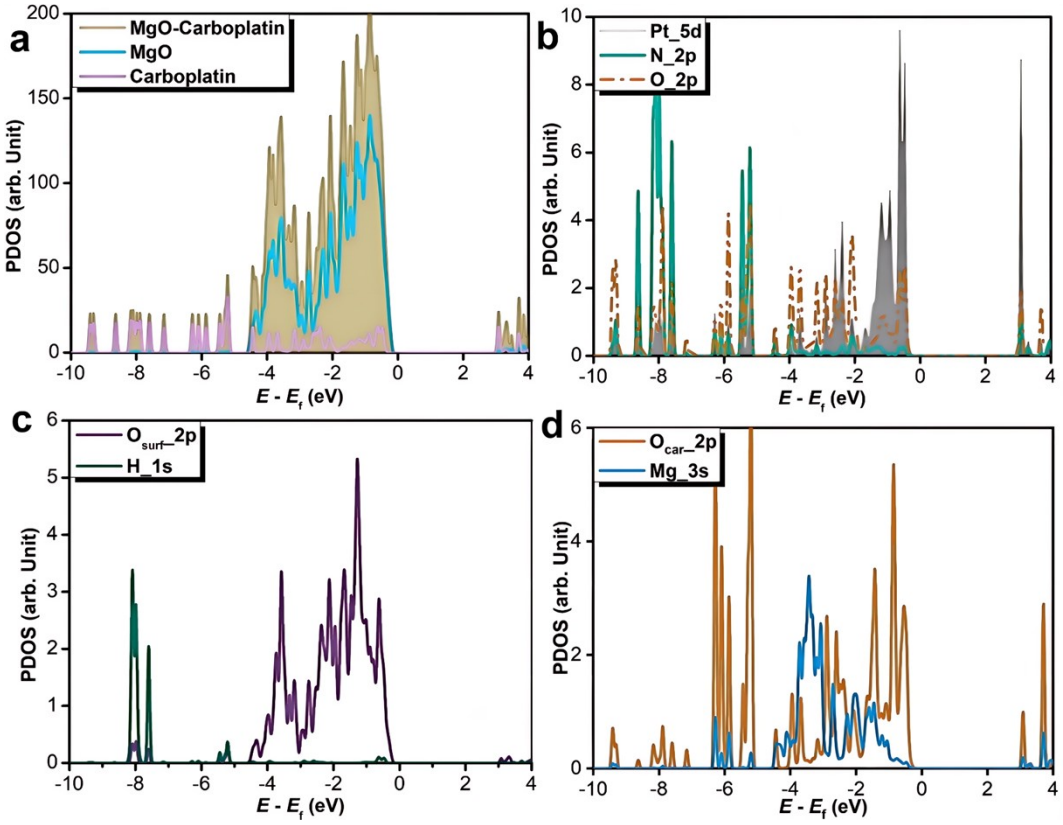

Fig. S5 The local projected density of states (PDOS) for carboplatin adsorption on magnesia (001). The energies are relative to the Fermi energy level (E_f).

Partial charge density (PCD) analysis from -0.5 eV to Fermi level, hydrolysis structure at hydroxylated MgO(100) sites, and Hydrolysis structure on MgO(100) film.

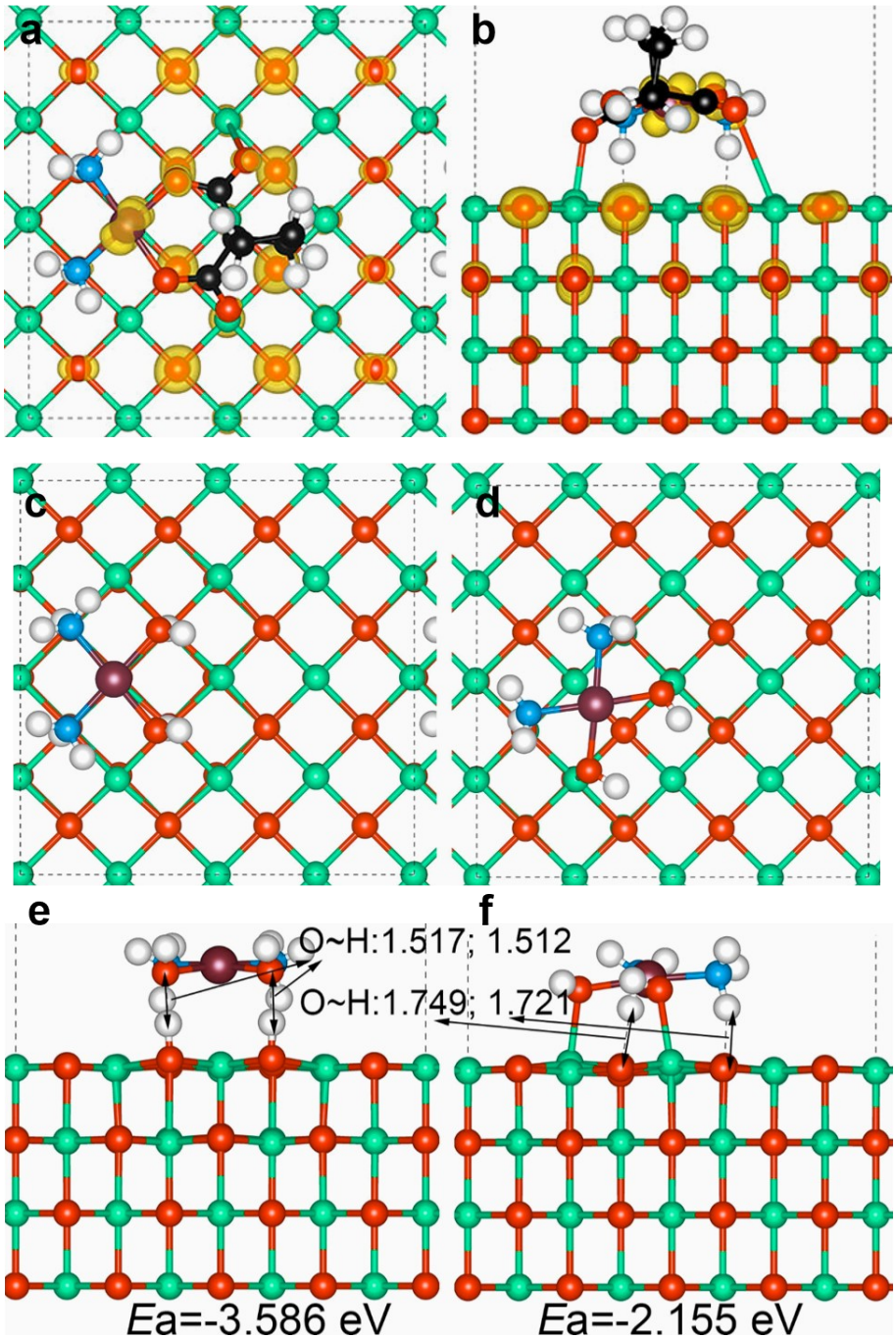

Fig. S6 (a,b) Partial charge density (PCD) analysis from -0.5 eV to Fermi level (isosurface: 0.02 e Bohr^{-3}); (c,e) Hydrolysis structure at hydroxylated MgO(100) sites; (d,f) Hydrolysis structure on MgO(100) film.

The projected electronic density of states (PDOS) for dispersed state of guanine base and the hydrolysis product

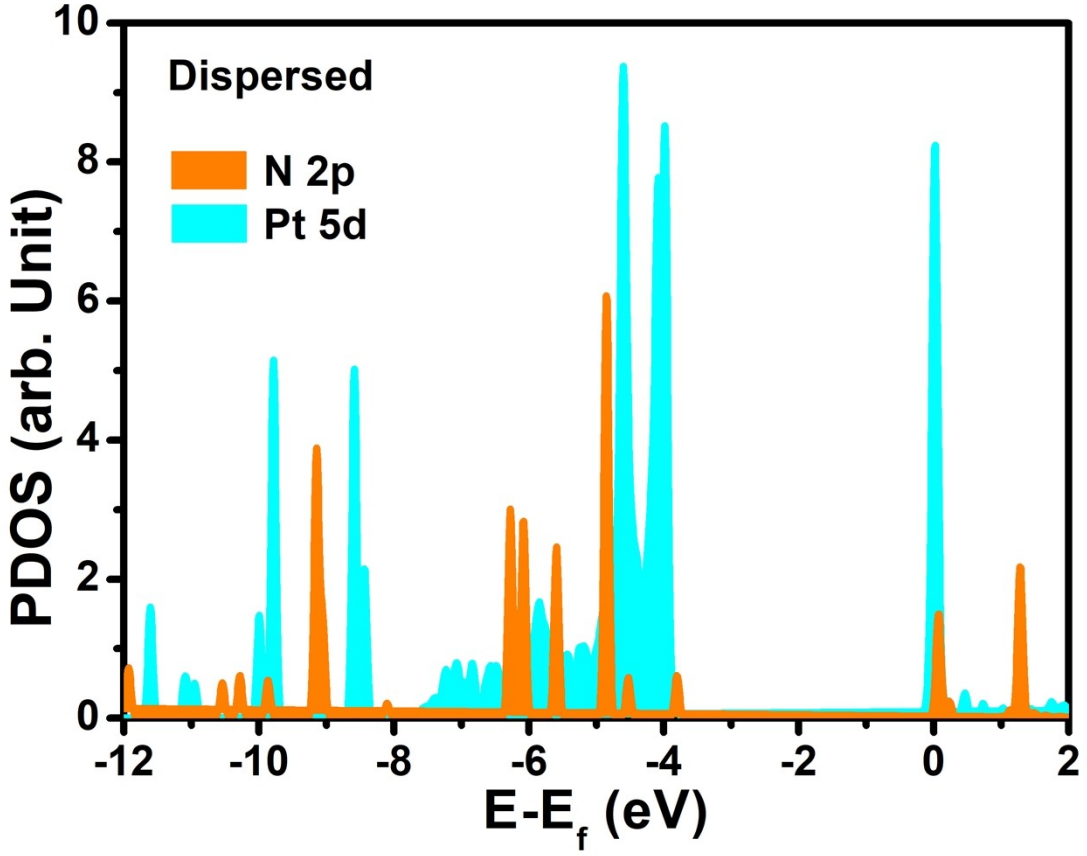

Fig. S7 The projected electronic density of states (PDOS) for dispersed state of guanine base and the hydrolysis product. The energy positions are taken relative to the Fermi energy level.

The projected electronic density of states (PDOS) for approaching state of guanine base and the hydrolysis product

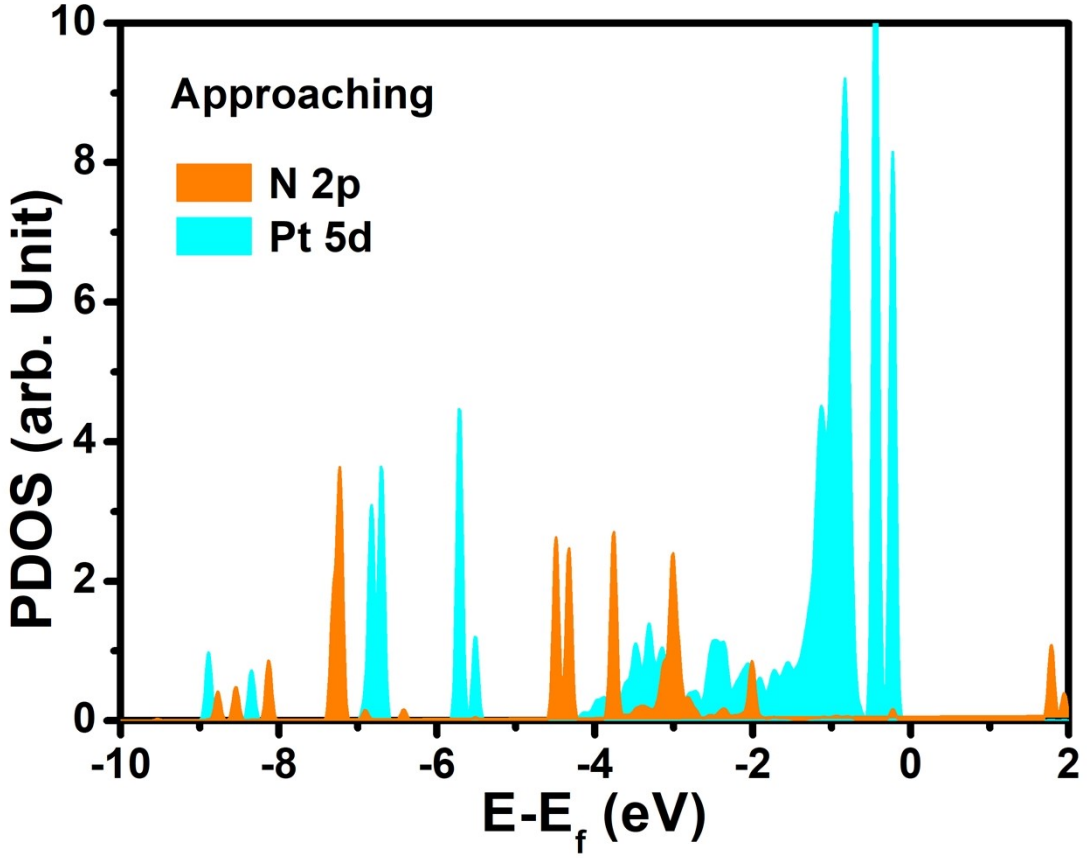

Fig. S8 The projected electronic density of states (PDOS) for approaching state of guanine base and the hydrolysis product. The energy positions are taken relative to the Fermi energy level.

The projected electronic density of states (PDOS) for combinating state of guanine base and the hydrolysis product

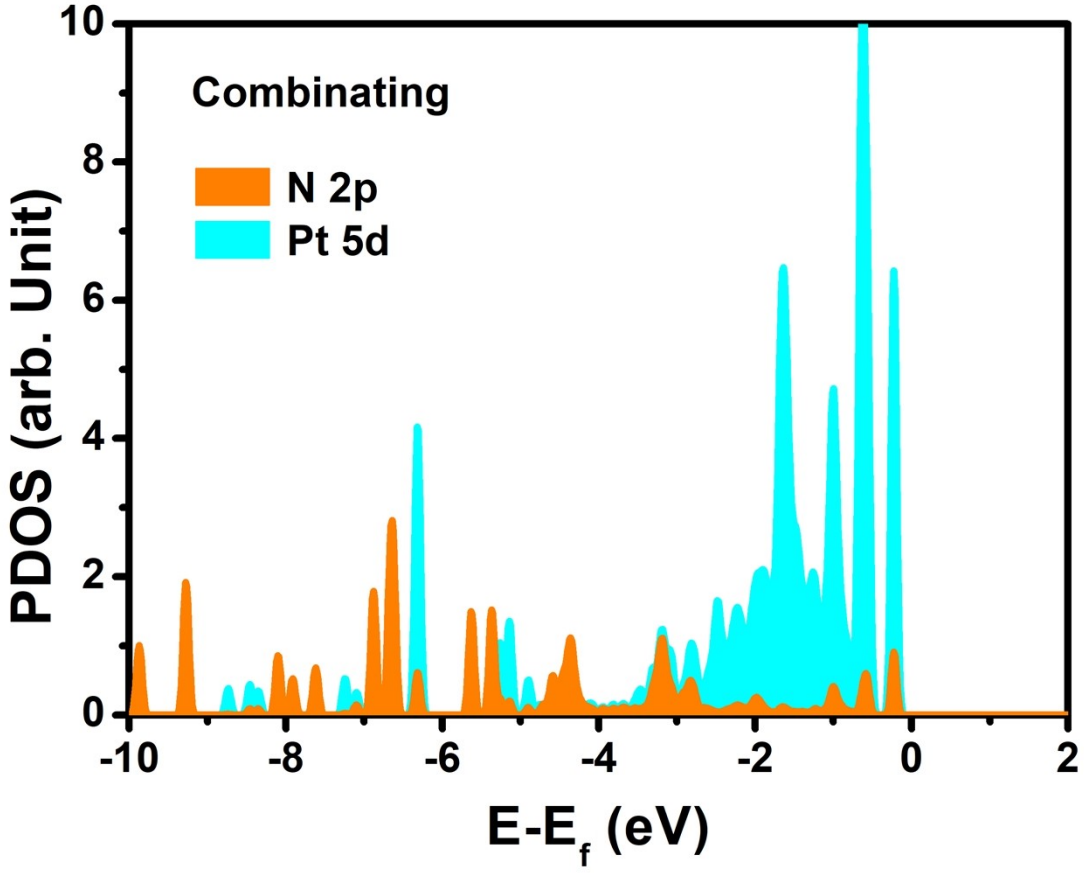

Fig. S9 The projected electronic density of states (PDOS) for combinating state of guanine base and the hydrolysis product. The energy positions are taken relative to the Fermi energy level.

Density evolution within 150 ps during the NPT process

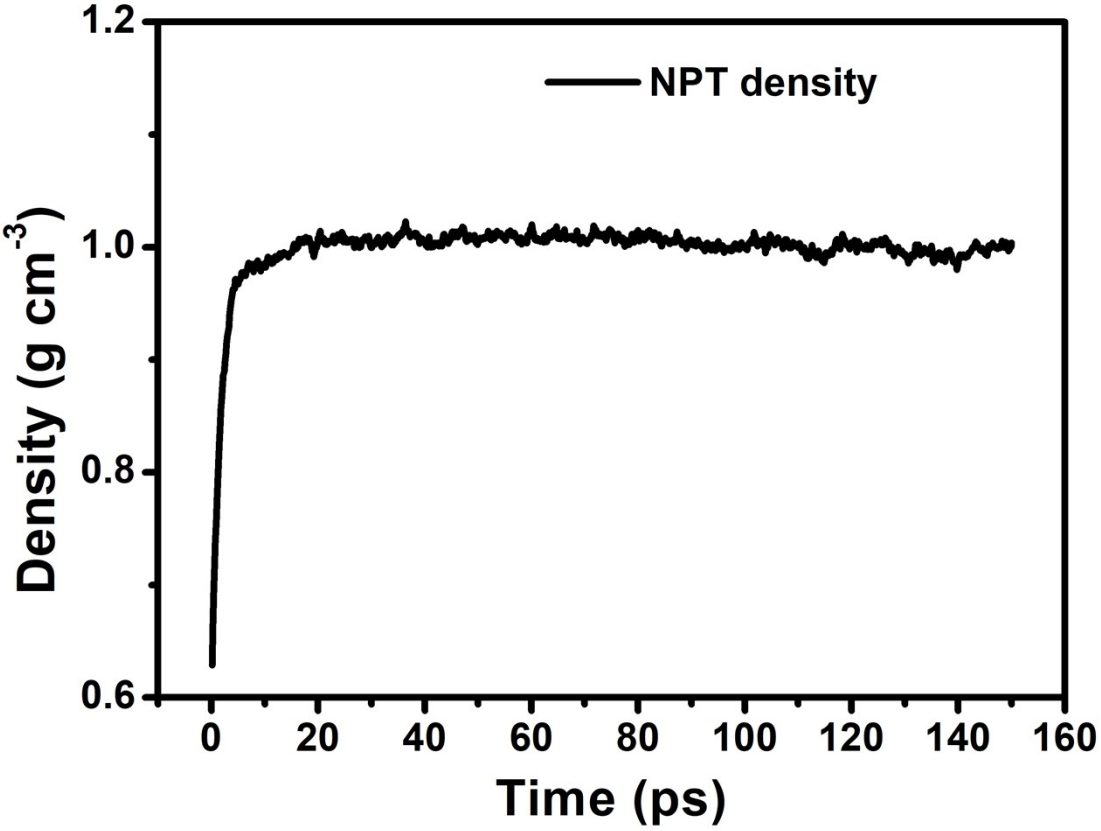

Fig. S10 Density evolution within 150 ps during the NPT process.

Temperature evolution within 150 ps during the NPT process

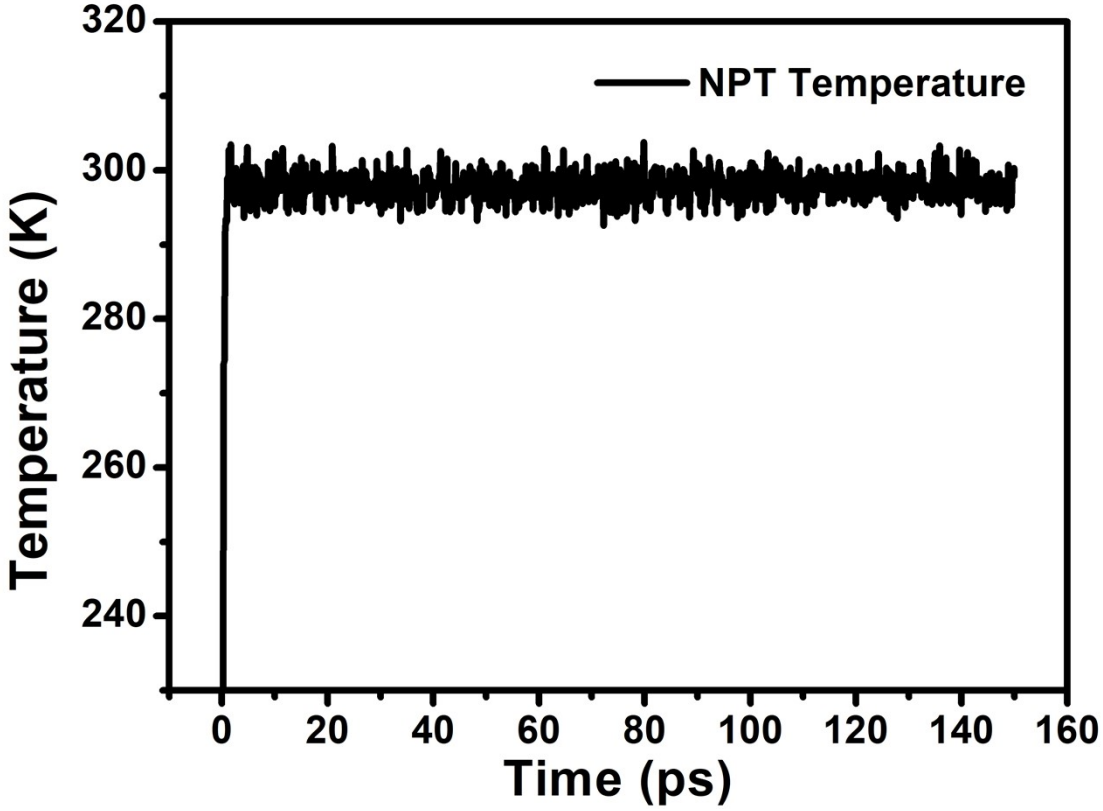

Fig. S11 Temperature evolution within 150 ps during the NPT process.

Temperature evolution within 1000 ps during the NVT process

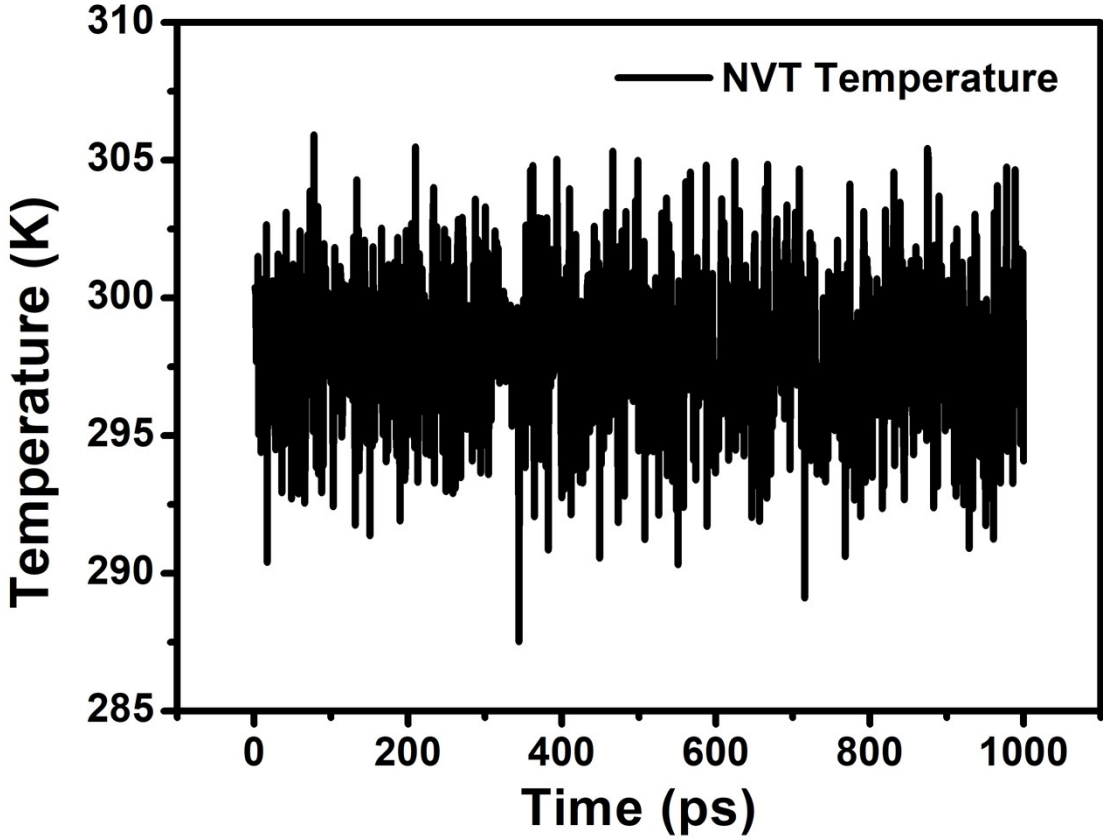

Fig. S12 Temperature evolution within 1000 ps during the NVT process.

Potential energy, kinetic energy, non-bond energy and total energy evolution within 1000 ps during the NVT process

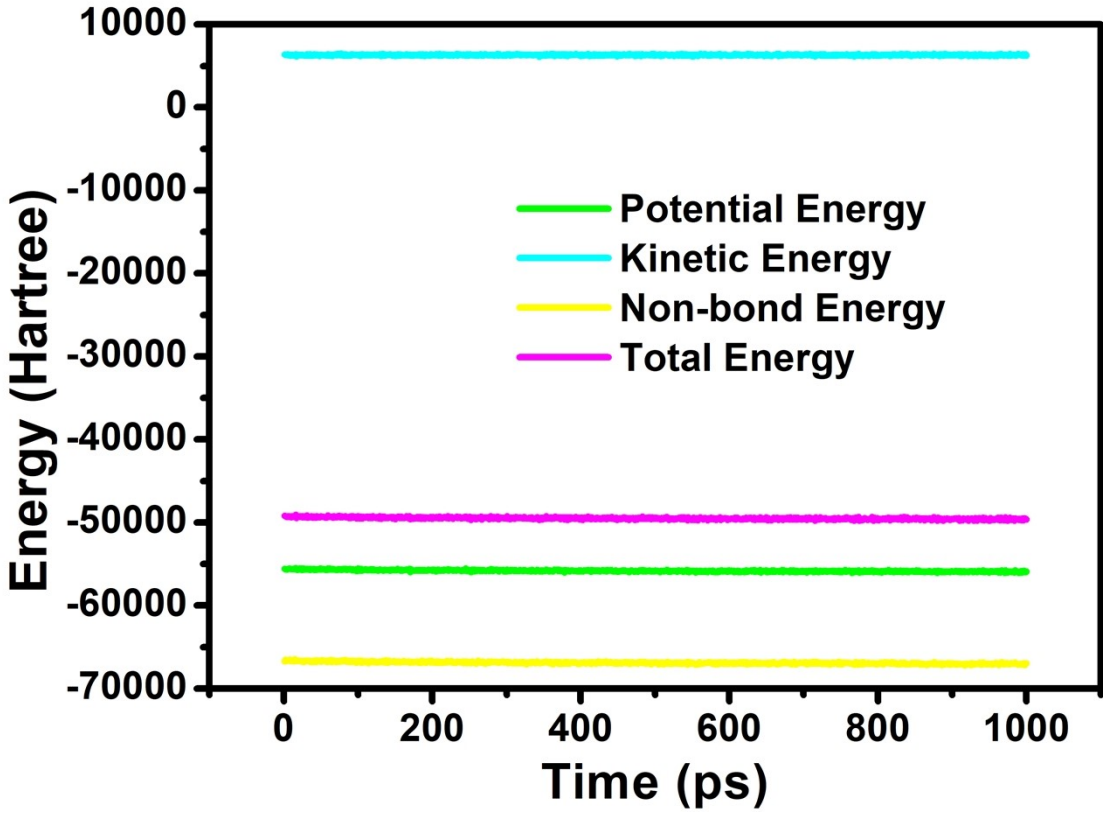

Fig. S13 Potential energy, kinetic energy, non-bond energy and total energy evolution within 1000 ps during the NVT process.

Time evolution of the Mean Square Displacement (MSD) during the molecular dynamics simulation

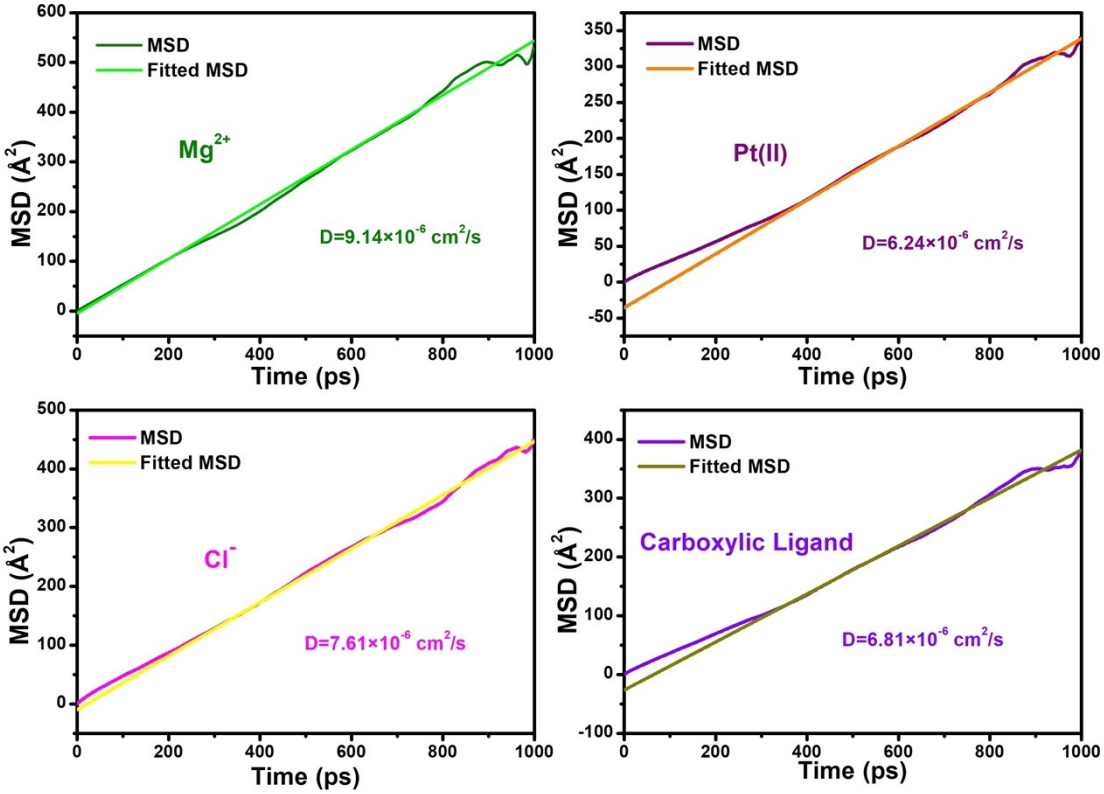

Fig. S14 Time evolution of the Mean Square Displacement (MSD) for Mg^{2+}, Pt(II), Cl^-, and the carboxylic ligand during the molecular dynamics simulation. The curved lines represent the calculated MSD data, while the straight lines denote the linear fitting used to derive the diffusion coefficients (D). The observed linear growth of MSD with time indicates that the system has reached an equilibrium diffusive state.

References

1. J. P. Perdew, K. Burke and Y. Wang, *Phys. Rev. B*, 1996, **54**, 16533-16539.
2. G. Kresse and J. Furthmüller, *Comput. Mater. Sci.*, 1996, **6**, 15-50.
3. J. P. Perdew, K. Burke and M. Ernzerhof, *Phys. Rev. Lett.*, 1996, **77**, 3865-3868.
4. S. Grimme, J. Antony, S. Ehrlich and H. Krieg, *J. Chem. Phys.*, 2010, **132**, 154104.
5. G. W. T. M. J. Frisch, H. B. Schlegel, G. E. Scuseria, M. A. Robb, J. R. Cheeseman, G. Scalmani, V. Barone, B. Mennucci, G. A. Petersson, H. Nakatsuji, M. Caricato, X. Li, H. P. Hratchian, A. F. Izmaylov, J. Bloino, G. Zheng, J. L. Sonnenberg, M. Hada, M. Ehara, K. Toyota, R. Fukuda, J. Hasegawa, M. Ishida, T. Nakajima, Y. Honda, O. Kitao, H. Nakai, T. Vreven, J. A. Montgomery, Jr., J. E. Peralta, F. Ogliaro, M. Bearpark, J. J. Heyd, E. Brothers, K. N. Kudin, V. N. Staroverov, T. Keith, R. Kobayashi, J. Normand, K. Raghavachari, A. Rendell, J. C. Burant, S. S. Iyengar, J. Tomasi, M. Cossi, N. Rega, J. M. Millam, M. Klene, J. E. Knox, J. B. Cross, V. Bakken, C. Adamo, J. Jaramillo, R. Gomperts, R. E. Stratmann, O. Yazyev, A. J. Austin, R. Cammi, C. Pomelli, J. W. Ochterski, R. L. Martin, K. Morokuma, V. G. Zakrzewski, G. A. Voth, P. Salvador, J. J. Dannenberg, S. Dapprich, A. D. Daniels, O. Farkas, J. B. Foresman, J. V. Ortiz, J. Cioslowski, and D. J. Fox, *Gaussian, Inc., Wallingford CT*, 2013.
6. Y. Zhang, B. Suo, Z. Wang, N. Zhang, Z. Li, Y. Lei, W. Zou, J. Gao, D. Peng, Z. Pu, Y. Xiao, Q. Sun, F. Wang, Y. Ma, X. Wang, Y. Guo and W. Liu, *J. Chem. Phys.*, 2020, **152**, 064113.
7. W. Liu, G. Hong, D. Dai, L. Li and M. Dolg, *Theor. Chem. Acc.*, 1997, **96**, 75-83.
8. W. Liu, F. Wang and L. Li, *J. Theor. Comput. Chem.*, 2003, **02**, 257-272.
9. R. Nelson, C. Ertural, J. George, V. L. Deringer, G. Hautier and R. Dronskowski, *J. Comput. Chem.*, 2020, **41**, 1931-1940.
10. S. Maintz, V. L. Deringer, A. L. Tchougréeff and R. Dronskowski, *J. Comput. Chem.*, 2016, **37**, 1030-1035.
11. Accelrys Software Inc., Material Studio Modeling Environment, 2020, Accelrys Software Inc., San Diego, Calif, USA.